Proceedings of ASME Turbo Expo 2014: Turbine Technical Conference and Exposition
GT2014
June 16 – 20, 2014, Düsseldorf, Germany

GT2014-27172

A MODEL-BASED ANOMALY DETECTION APPROACH FOR ANALYZING STREAMING AIRCRAFT ENGINE MEASUREMENT DATA

Donald L. Simon
NASA Glenn Research Center
21000 Brookpark Road
Cleveland, OH, 44135

Aidan W. Rinehart
Vantage Partners, LLC
3000 Aerospace Parkway
Brook Park, OH 44142

ABSTRACT

This paper presents a model-based anomaly detection architecture designed for analyzing streaming transient aircraft engine measurement data. The technique calculates and monitors residuals between sensed engine outputs and model predicted outputs for anomaly detection purposes. Pivotal to the performance of this technique is the ability to construct a model that accurately reflects the nominal operating performance of the engine. The dynamic model applied in the architecture is a piecewise linear design comprising steady-state trim points and dynamic state space matrices. A simple curve-fitting technique for updating the model trim point information based on steady-state information extracted from available nominal engine measurement data is presented. Results from the application of the model-based approach for processing actual engine test data are shown. These include both nominal fault-free test case data and seeded fault test case data. The results indicate that the updates applied to improve the model trim point information also improve anomaly detection performance. Recommendations for follow-on enhancements to the technique are also presented and discussed.

NOMENCLATURE

C-MAPSS40k	Commercial modular aero-propulsion system simulation, 40k
FDI	fault detection and isolation
FOQA	flight operations quality assurance
PBM	performance baseline model
PWLM	piecewise linear model
RTSTM	real-time self-tuning model
WSSR	weighted sum of squared residuals
VIPR	vehicle integrated propulsion research

INTRODUCTION

Aircraft operators rely on engine condition monitoring and gas path fault diagnostics to help ensure the safe and efficient operation of their gas turbine engine assets. A typical architecture depicting this functionality is shown in Fig. 1. As shown, this architecture includes both on-board and ground-based functionality. On-board fault detection and isolation (FDI) logic continuously monitors control sensors and actuators. Additionally, automated data acquisition logic is applied to collect in-flight engine measurements. These engine measurements, along with any identified engine fault conditions identified by the on-board FDI logic, are transmitted off-board to fleet-wide ground stations that apply additional monitoring functionality. Conventionally, ground-based gas path diagnostic approaches are designed to analyze steady-state snapshot engine measurement data collected at a limited number of discrete operating points each flight. Early diagnosis of incipient fault conditions with minimal latency is challenging. However, advances in on-board processing and flight data recording capabilities are enabling the acquisition of full-flight streaming, or continuous, measurement data. This includes flight operation quality assurance (FOQA) and flight data monitoring programs implemented by airlines [1,2]. Such data span a broad range of aircraft flight conditions including transient engine operating scenarios. An example of aircraft engine flight data is shown in Fig. 2. This figure shows full-flight data, which contains considerable transients, along with notional conventional snapshot measurement points. While this vastly expanded quantity of engine data presents new diagnostic opportunities, it also necessitates the development of new analysis approaches that account for the expanded quantity and dynamic content of the data. As the volume and availability of flight datasets continues to increase, the future emphasis on using these databases for performance and condition monitoring purposes is also expected to grow.

In response to the need for new methods for analyzing aircraft flight data for health monitoring purposes, several research efforts in this area have been conducted within the aviation community. Chu and Gorinevsky have presented work on aircraft anomaly detection techniques applied for processing FOQA data [3,4], and Das *et al* have presented a data driven approach for anomaly detection in flight recorder data [5].

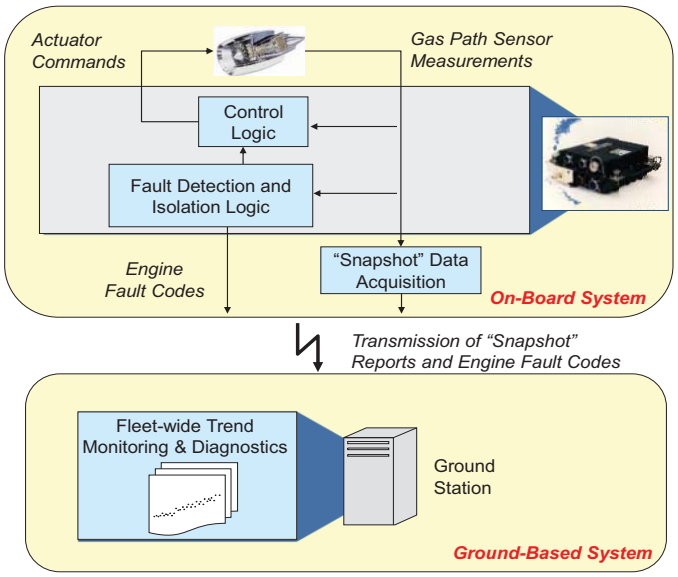

Figure 1. Conventional aircraft engine condition monitoring and gas path fault diagnostic architecture.

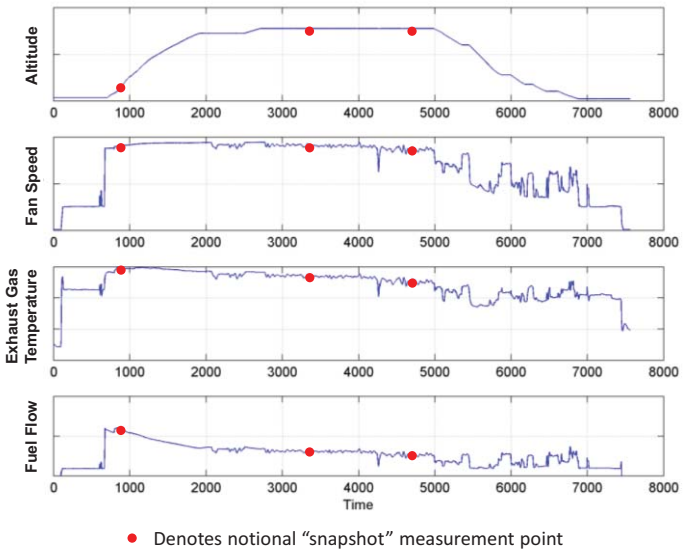

Figure 2. Example commercial aircraft engine flight data.

Merrington *et al* applied analytical redundancy methods to process aircraft gas turbine engine transient measurement data [6], and Kerr *et al* [7], Dewallef *et al* [8], and Borguet *et al* [9] have each proposed Kalman filter-based approaches for the on-line processing of aircraft engine measurement data for diagnostic purposes.

Recently, NASA developed a unified approach for processing full-flight streaming engine data for performance estimation and fault diagnostic purposes [10,11]. This model-based approach is suitable for either post-flight or on-board processing of acquired engine flight data. Simulation studies have found this architecture to hold promise for analyzing streaming flight data either in real-time or post-flight. However, key to the performance of this or any other model-based diagnostic technique is having a model that accurately reflects the nominal operating performance of the actual engine. Often, available engine models do not match the actual engine well due to modeling inaccuracies, or unaccounted enhancements, or configuration changes an engine design may undergo over its lifecycle. These issues can negatively impact the performance of model-based diagnostic approaches. In Ref. [12] a hybrid modeling approach is applied combining analytical and empirical modeling to achieve improved model-to-engine matching. The empirical component of this hybrid model is based on a neural network trained to learn observed residuals between the engine and the model based on available engine measurement data. This has been shown to improve model-to-engine matching, but only addresses the portion of the engine operating envelope from which measurement data is available for training the neural network. The study presented in this paper addresses engine-to-model inaccuracies by applying a simple curve fitting technique for updating the model based on steady-state information extracted from nominal engine measurement data. Furthermore, the identified curve fits can be readily extended (extrapolated) to additional portions of the operating envelope beyond that from which measurement data is available. This technique has been found to improve overall model accuracy and enable successful anomaly detection when implemented within the NASA-developed model-based diagnostic architecture.

The paper is organized as follows. First, the NASA-developed model-based architecture for integrated aircraft engine performance estimation and fault diagnostics is presented. This is followed by a description of model enhancements made to improve engine-to-model matching based on available nominal engine measurement data. Next, the architecture is applied to analyze actual engine test data including both nominal and faulty engine operating scenarios. The architecture's anomaly detection performance with and without the model enhancements are presented and compared. This is followed by a discussion of potential follow-on work and conclusions.

MODEL-BASED ARCHITECTURE FOR PROCESSING STREAMING AIRCRAFT ENGINE MEASUREMENT DATA

The NASA-developed model-based architecture for integrated aircraft engine performance estimation and fault diagnostics is shown in Fig. 3. It contains two models designed to operate in parallel—a real-time self-tuning model (RTSTM) and a performance baseline model (PBM). The RTSTM is a self-tuning engine model based on a piecewise linear Kalman filter. It self-tunes to account for performance deterioration that the engine may incur over time with usage. The RTSTM is capable of providing real-time estimates of measured and unmeasured engine performance parameters for condition monitoring purposes. The PBM is designed to provide a reference baseline of recent past engine performance. It incorporates a version of the same piecewise linear model used

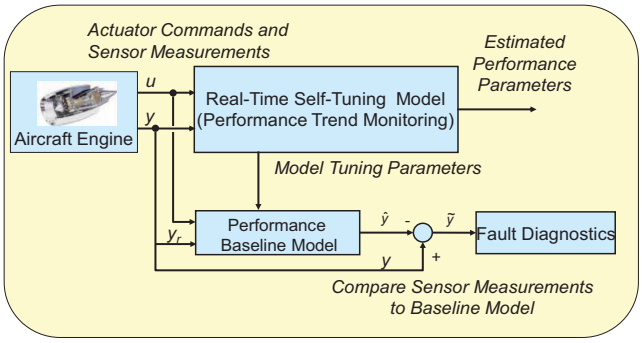

Figure 3. Performance trend monitoring and gas path fault diagnostic architecture

in implementing the RTSTM. The PBM accepts inputs consisting of actuator commands, u, and a parameter representative of engine power, y_r, such as fan speed or engine pressure ratio. The PBM is driven to the power reference parameter to prevent the model from inadvertently diverging from the engine. In addition to receiving continuous inputs from the engine, the model also automatically receives periodically updated tuning parameter estimates from the RTSTM. This periodic update of the tuning parameters allows the PBM to adapt to normal performance deterioration that occurs gradually over time, but prevents the model from immediately adapting to rapid performance shifts caused by faults. The frequency of the periodic tuning parameter update is user-specified, but is recommended to be on the order of once per flight. Sensed engine outputs, y, and PBM predicted engine outputs, $\hat{y}$, are compared, and the resulting residual vector, $\tilde{y}$, is analyzed for diagnostic purposes. Small residuals indicate that the engine is operating nominally, whereas large residuals indicate anomalous engine behavior.

The subsections below will first discuss the construction of a piecewise linear model used to implement the RTSTM and PBM, followed by a description of the anomaly detection logic applied within the performance trend monitoring and gas path diagnostic architecture. This is followed by a description of the enhancements made to help improve model-to-engine matching.

Piecewise Linear Model Implementation

An aircraft engine piecewise linear model (PWLM) is created from an available transient nonlinear engine model, or cycle deck. Linear state space system point models are extracted from the nonlinear model and then combined and scheduled for interpolation based on engine operating point. In this fashion the PWLM is able to approximate the transient full-envelope nonlinear model response, while offering advantages over the more complex nonlinear model. A PWLM is usually less computationally intensive than its nonlinear equivalent, and the simpler structure allows for straightforward design of linear estimation approaches such as a Kalman filter. A detailed description of PWLM construction can be found in Ref. [13], and is summarized below.

The nonlinear model of an aircraft engine is assumed to be represented by the following equations

$$\begin{aligned} \dot{x} &= f(x,u,h) \\ y &= g(x,u,h) \end{aligned} \tag{1}$$

where x and u represent the vectors of engine state variables and control command inputs, respectively. The vector h represents health parameters, such as efficiency or flow capacity, reflective of performance deterioration within the major rotating modules of the engine. For given input values, the nonlinear functions f and g generate the vectors of state derivatives $\dot{x}$, and sensed engine outputs y, respectively. By linearizing the engine model at a given operating point, the following state-space equations can be obtained:

$$\begin{aligned} \dot{x} &= A\underbrace{(x - x_{trim})}_{\Delta x} + B\underbrace{(u - u_{trim})}_{\Delta u} + L\underbrace{(h - h_{ref})}_{\Delta h} \\ \dot{x} &= A\Delta x + B\Delta u + L\Delta h \\ \underbrace{y - y_{trim}}_{\Delta y} &= C\underbrace{(x - x_{trim})}_{\Delta x} + D\underbrace{(u - u_{trim})}_{\Delta u} + M\underbrace{(h - h_{ref})}_{\Delta h} \\ \Delta y &= C\Delta x + D\Delta u + M\Delta h \end{aligned} \tag{2}$$

Here, A, B, C, D, L, and M are the state-space matrices reflecting system dynamics. The trim vectors, denoted by the subscript "*trim*," reflect the values of the state variables, commands, and sensed outputs when the model is at steady-state (i.e., $\dot{x} = 0$) at the given operating point. Collectively, the trim vectors define what is referred to as a "trim point." The vector h_{ref} represents a reference health condition specified by the system designer. In Eq. (2), parameter deviations relative to trim or reference conditions are denoted by the delta symbol (Δ). A block diagram illustration of the linear state space model implementation at a single operating point is shown in Fig. 4.

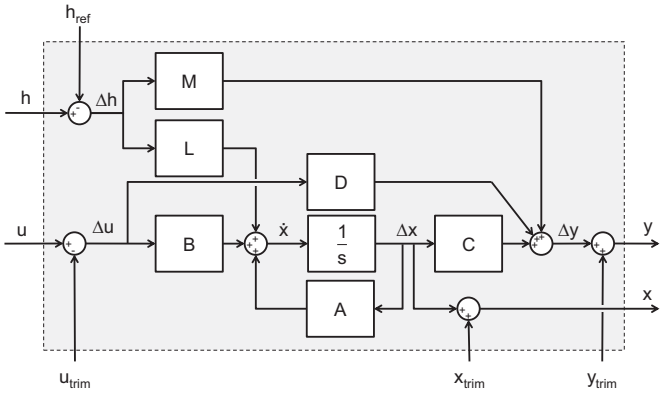

Figure 4. Linear state-space model implementation

The initial step in creating this PWLM is the computation of linear state-space models from the nonlinear model at multiple operating points. These operating points serve as the interpolation scheduling parameters in the piecewise linear model. Figure 5 shows a notional three-dimensional example of operating point specification using altitude, Mach number, and power setting as the scheduling parameters. The number of operating points and spacing between operating points, which does not have to be uniform, are design decisions left to the end user.

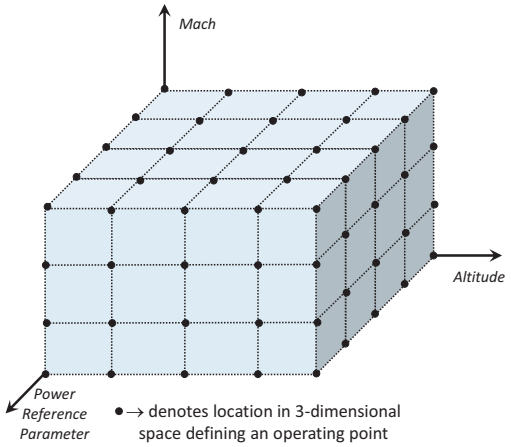

Figure 5. Example of three-dimensional piecewise linear model operating point scheduling

Anomaly Detection

Within the model-based diagnostic architecture, anomaly detection is performed by monitoring residuals between sensed engine outputs and those predicted by the performance baseline model (See Fig. 3). If no fault is present, the engine and PBM are expected to be in good agreement, in which case the residuals will be small. Conversely, in the event of a system fault impacting engine performance, the engine and PBM will diverge and the residuals will increase. Anomaly detection is performed by monitoring a weighted sum of squared residuals (WSSR), which is calculated as shown in Eq. (3)

$$\mathrm{WSSR} = \tilde{y}^T R^{-1} \tilde{y} \qquad (3)$$

Here, $\tilde{y}$ is the vector of measurement residuals reflecting the difference between sensed engine outputs and PBM produced outputs and R is the sensor measurement covariance matrix. If necessary, the WSSR signal can be filtered to smooth the signal and eliminate any short-term outliers contained therein. The WSSR signal is compared against a defined threshold, and if that threshold is exceeded an anomaly is declared.

Re-trimming of Piecewise Linear Model

As mentioned previously, a model's ability to accurately reflect the sensed outputs of the actual engine is key in enabling effective model-based diagnostic methods based on that model. The step taken in this study to improve engine-to-model steady-state matching is to "re-trim" the PWLM based on nominal steady-state engine data extracted from engine flight data or test cell data. Re-trimming the model entails adjusting the u_{trim} and y_{trim} vectors along with any sensed elements of the x_{trim} vector shown in Eq. (2) to match the acquired steady-state data. The re-trimming process is envisioned to occur at relatively infrequent intervals, for example, when an engine first enters into service or undergoes a major overhaul. Additionally, for on-board applications this is not intended to occur on-board the aircraft. Rather, the intent is for the model to be re-trimmed off-line (off-board), and then loaded into an on-board processor. The steps in the re-trimming process include identifying engine steady-state operating points over a range of power settings, applying a polynomial curve fit to that data, and adjusting the model trim vector information to match the polynomial curve fit. Each step is further discussed below.

Identification of engine steady-state operating points. In this study, steady-state engine operating performance is approximated based on streaming engine measurement data acquired under known nominal (fault-free) conditions from a single engine. A fixed-time length sliding window approach is applied to analyze the data and determine whether each individual sample of measurement data is reflective of steady-state engine operation. Several criteria must be met to satisfy the steady-state assumption. First, engine operating conditions (e.g., pressure altitude and Mach number) must remain within defined ranges over the past fixed-time window. Second, the standard deviation of select engine measurement parameters in the window must be below defined thresholds. Finally, the absolute difference between the current sample and the mean within the window for select engine measurement parameters must be below defined thresholds. If all of these criteria are met, the engine is assumed to be at steady-state and the current vector of measurement data is archived for subsequent use in obtaining the polynomial curve fits that will be used for re-trimming the model. The sliding window is then advanced forward one time step and the process is repeated on the next data point.

Polynomial curve fit. Given the acquired engine steady-state data within a fixed pressure altitude and Mach number range, the next step is to apply a curve fit through each measured parameter plotted against the engine power reference parameter used in the PWLM. This power reference parameter is typically a parameter such as corrected fan speed or engine pressure ratio. At any arbitrary steady-state sample k, an n^{th} order polynomial equation expressing a measured engine output, y_i, as a function of the engine power reference parameter, y_r, can be written as

$$y_{i,k} = p_{i,0} + p_{i,1} y_{r,k} + p_{i,2} y_{r,k}^2 + \cdots + p_{i,n} y_{r,k}^n \qquad (4)$$

where $p_{i,0}$, $p_{i,1}$, $p_{i,2}$, …, $p_{i,n}$ are the polynomial coefficients. Assuming N steady-state samples have been identified, the

polynomial equations for these samples can be concatenated as shown in Eq. (5)

$$\begin{bmatrix} y_{i,1} \\ y_{i,2} \\ \vdots \\ y_{i,k} \\ \vdots \\ y_{i,N} \end{bmatrix} = \begin{bmatrix} p_{i,0} + p_{i,1}y_{r,1} + p_{i,2}y_{r,1}^2 + \cdots + p_{i,n}y_{r,1}^n \\ p_{i,0} + p_{i,1}y_{r,2} + p_{i,2}y_{r,2}^2 + \cdots + p_{i,n}y_{r,2}^n \\ \vdots \\ p_{i,0} + p_{i,1}y_{r,k} + p_{i,2}y_{r,k}^2 + \cdots + p_{i,n}y_{r,k}^n \\ \vdots \\ p_{i,0} + p_{i,1}y_{r,N} + p_{i,2}y_{r,N}^2 + \cdots + p_{i,n}y_{r,N}^n \end{bmatrix} \tag{5}$$

Applying algebraic manipulation, Eq. (5) can be written as

$$\underbrace{\begin{bmatrix} y_{i,1} \\ y_{i,2} \\ \vdots \\ y_{i,k} \\ \vdots \\ y_{i,N} \end{bmatrix}}_{Y_i} = \underbrace{\begin{bmatrix} 1 & y_{r,1} & y_{r,1}^2 & \cdots & y_{r,1}^n \\ 1 & y_{r,2} & y_{r,2}^2 & \cdots & y_{r,2}^n \\ \vdots & \vdots & \vdots & \vdots & \vdots \\ 1 & y_{r,k} & y_{r,k}^2 & \cdots & y_{r,k}^n \\ \vdots & \vdots & \vdots & \vdots & \vdots \\ 1 & y_{r,N} & y_{r,N}^2 & \cdots & y_{r,N}^n \end{bmatrix}}_{H_r} \underbrace{\begin{bmatrix} p_{i,0} \\ p_{i,1} \\ p_{i,2} \\ \vdots \\ p_{i,n} \end{bmatrix}}_{P_i} \tag{6}$$

$$Y_i = H_r P_i$$

where Y_i is an $N\times1$ vector of steady-state measurements for parameter y_i, P_i is an nx1 vector of polynomial coefficients, and H_r is an $N\times n$ matrix relating P_i to Y_i. An estimate of the vector of polynomial coefficients, $\hat{P}_i$, can be obtained applying a least squares solution as shown in Eq. (7)

$$\hat{P}_i = \left(H_r^T H_r\right)^{-1} H_r^T Y_i \tag{7}$$

A notional illustration of a polynomial curve fit through acquired steady-state data is shown in Fig. 6. Here, a single engine output, y_i, is plotted against the power reference parameter, y_r. The red line represents the y_i vs. y_r curve based on trim point information contained in the original piecewise linear model, the black "x's" represent steady-state operating points based on actual sensed engine data, and the blue curve is the polynomial curve fit through those steady-state points. Note that the polynomial curve fit provides a better representation of actual engine performance compared to that of the original model. It is noted that Eqs. (4)-(7) only illustrate the polynomial curve fitting process for a single element (i.e., the i^{th} element) of the sensed measurement trim vector, y_{trim}. Although not shown, an analogous set of equations are also produced and applied in order to construct unique curve fits for each additional element of the piecewise linear model y_{trim} vector, each element of the u_{trim} vector, and any sensed elements of the x_{trim} vector. Furthermore, for an individual actuator command or state variable, the y_i information shown in Eqs. (4)-(7) is replaced with u_i or x_i, respectively.

A necessity for constructing accurate curve fits is the need for a suitable amount of steady-state data points distributed across a broad range of engine power settings. If most of the steady-state data points are concentrated in a narrow y_r range it will be difficult to obtain curve fits that reflect the true performance of the engine.

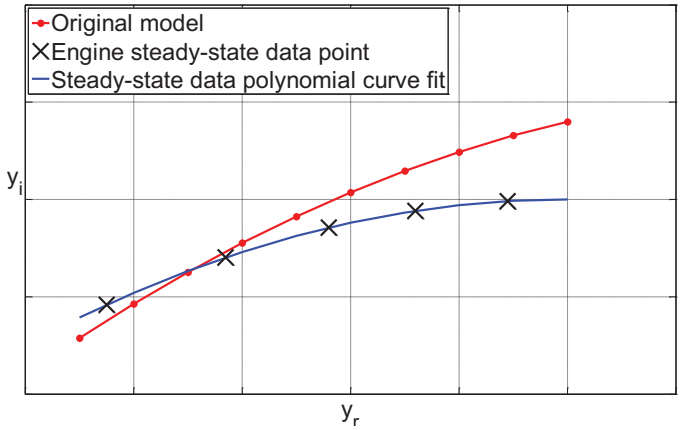

Figure 6. Illustration of steady-state data polynomial curve fit

Adjusting model trim points. Once polynomial curve fits have been identified for each parameter, that information is used to adjust, or "re-trim," the piecewise linear model trim points. This is illustrated in Fig. 7. Here, the solid red and blue lines represent the original and the re-trimmed y_i vs. y_r curves for the given altitude and Mach number range where the steady-state data points were obtained. The lighter dashed lines represent curves at additional altitude and Mach numbers. If sufficient steady-state data is available, curve fits may be performed at different altitude and Mach number combinations. However, for those altitude and Mach numbers where steady-state data is limited or unavailable, y_i vs. y_r curves can be approximated based on a curve fit performed at another operating point. This is done by first applying a least squares calculation to determine a scale factor and offset reflecting the separation between two y_i vs. y_r curves in the original model—specifically, the separation between a curve where steady-state data is available (solid red line in Fig. 7) and a second curve at the altitude and Mach number where steady-state data is unavailable (a dashed red line in Fig. 7). Next, the obtained scale factor and offset is applied to adjust the re-trimmed model y_i vs. y_r curve (solid blue line in Fig. 7) by a proportionate amount, thus enabling the calculation of a re-trimmed model y_i vs. y_r curve at the corresponding altitude and Mach number (a dashed blue line in Fig. 7). This process is repeated to calculate and apply a unique scale factor and offset adjustment for each y_i vs. y_r curve at each altitude and Mach number combination in the model.

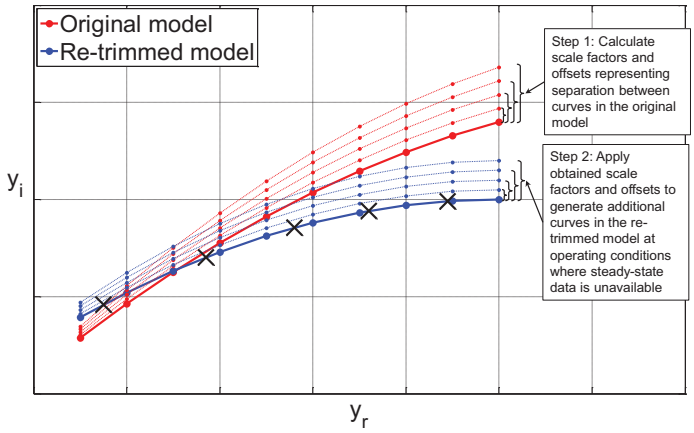

Figure 7. Illustration of re-trimmed piecewise linear model

APPLICATION EXAMPLE

In this section, an example application of the model-based anomaly detection architecture processing actual engine test data is presented. This example demonstrates the processing of data acquired during the NASA Vehicle Integrated Propulsion Research (VIPR) test program—a ground test conducted at NASA Dryden Flight Research Center and the Edwards Air Force Base on a C-17 aircraft equipped with Pratt & Whitney F117 turbofan engines. An objective of the VIPR program is to develop and demonstrate engine health management technologies including advanced sensors and diagnostic algorithms. The VIPR program included both nominal (fault-free) and non-damaging seeded fault engine test scenarios.

The engine gas path sensor measurements and actuator commands acquired during the VIPR testing are shown in Table 1 and Table 2, respectively. The model-based anomaly detection architecture, shown in Fig. 3, was designed and applied for processing this data. This architecture was developed using the NASA C-MAPSS40k turbofan engine model [14]. While of the same thrust category as the Pratt & Whitney F117 turbofan engines used in the VIPR test, C-MAPSS40k is not the same engine and therefore notable engine-to-model mismatches exist. As such, updating of the model is necessary to achieve suitable matching with the engines. The subsections below will first discuss re-trimming of the piecewise linear model and then show anomaly detection and RTSTM Kalman filter tuning parameter estimation results obtained by updating the model.

Table 1. Gas Path Sensor Measurements

Symbol	Description
N1	fan speed
N2	core speed
Ps3	high pressure compressor exit static pressure
T35	high pressure compressor exit total temperature
P5	low pressure turbine exit total pressure
T5	low pressure turbine exit total temperature

Table 2. Actuator Commands

Symbol	Description
Wf	fuel flow
VSV	variable stator vanes
BLD25	station 2.5 bleed valve
BLD14	14^{th} stage bleed valve

Re-trimming of Piecewise Linear Model

The first step in re-trimming the model is to identify steady-state data points within the available nominal (fault-free) data. During the VIPR test, several fault-free "baseline" runs were conducted where the engine was operated over a range of power settings spanning idle to max power. Figure 8 shows the time history of one of the engine gas path measurement parameters acquired during a VIPR test baseline run. In this figure, and all other figures in this section of the paper, units have been omitted and y-axis parameter names are simply referred to as y_i to protect the proprietary nature of the data. As shown in Fig. 8, the baseline run consists of a series of steady-state stair steps in power settings starting at idle, stepping up to max power, and then stepping back down to idle. The steady-state stair steps are then followed by a gradual acceleration/deceleration (idle-max-idle), and then a rapid acceleration/deceleration (idle-max-idle). In the figure, the blue line represents the acquired raw data and the red dots represent identified steady-state data points. Here, the steady-state criteria was defined as a data point where the standard deviation of both N1 and N2 is below 25 rpm based on a 100 second window of past data and the absolute residual between the current data point and the mean value over past 100 second window of N1 and N2 is less than 20 rpm. If these criteria are all met the engine is assumed to be at steady-state.

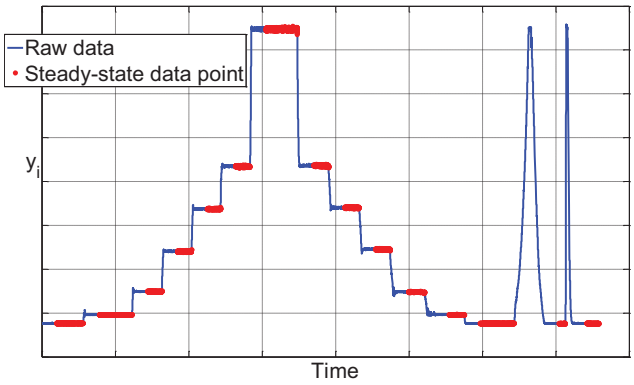

Figure 8. Example of steady-state data points identified within a baseline run

Figures 9 and 10 show example steady-state y_i vs. y_r curves for two of the acquired engine gas path parameters. Here, corrected fan speed is used as the power reference parameter, y_r, and the y_i parameters are labeled as y_a and y_b in Figs. 9 and 10, respectively. Each figure shows the original C-MAPSS40k generated curves (red line), steady-state data points identified from VIPR nominal baseline runs (black "X's"), and a fourth

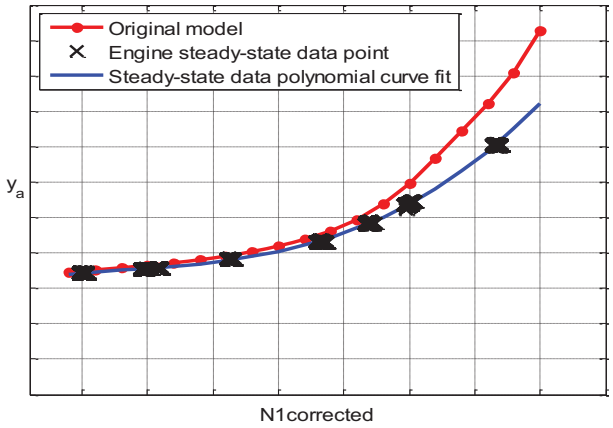

Figure 9. Original model and polynomial curve fit through steady-state data (parameter y_a)

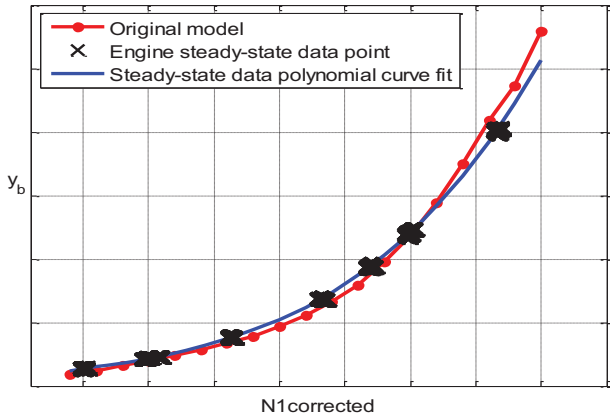

Figure 10. Original model and polynomial curve fit through steady-state data (parameter y_b)

order polynomial curve fit through the acquired steady-state data points (blue line). The order of this curve fit was determined manually through trial and error. As seen in these figures, the original piecewise linear model based on C-MAPSS40k does not match the steady-state performance of the actual engine. However, the polynomial curve fit is able to match the steady-state data points fairly well.

Since the VIPR test was a ground test all of the data was acquired at zero Mach and approximately the same pressure altitude. Figures 11 and 12 illustrate the extension of the data collected at this operating point to other altitude and Mach numbers for the purpose of re-trimming the entire piecewise linear model. All parameters are shown as corrected parameters. Since the VIPR data exhibited no Mach number variation and limited pressure altitude variation, it was not possible to validate whether the re-trimmed model accurately matched the actual engine over the entire operating envelope. However, this will be assessed in future studies focused on the processing of actual engine flight data spanning a broad operating range of altitudes and Mach numbers.

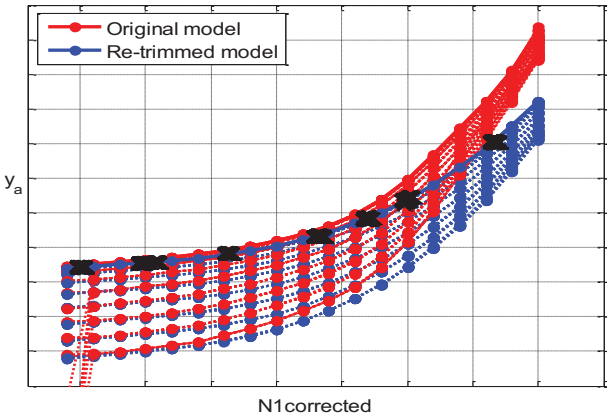

Figure 11. Original and re-trimmed PWLM (parameter y_a)

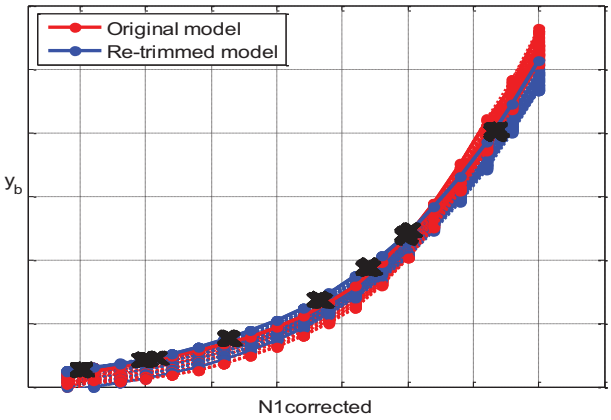

Figure 12. Original and re-trimmed PWLM (parameter y_b)

Residual Calculation

The model-based anomaly detection architecture was updated to use the re-trimmed piecewise linear model design. Then, both nominal and faulty data acquired during the VIPR testing was supplied as input to the architecture. Figures 13 and 14 show the benefit of using the re-trimmed piecewise linear model compared to the original piecewise linear model for processing nominal fault-free data acquired during two of the VIPR baseline runs. The top half of each figure shows information for one of the engine sensed gas path parameters, y_i, including the actual engine measurement (green line), the estimated value produced by the original PBM model (red line), and the estimated value produced by the re-trimmed PBM model (blue line). Note that the engine measurement (green line) is partially obscured by the re-trimmed PBM (blue line) in these plots. The bottom half of each figure shows the y_i residual between the engine measurement and the original PBM (red line) and the re-trimmed PBM (blue line). For both of the baseline runs, the re-trimmed model provides much better matching with the actual engine, which is desired in these cases where no fault is present. Conversely, the original model exhibits a large amount of mismatch, which limits its utility for fault detection purposes.

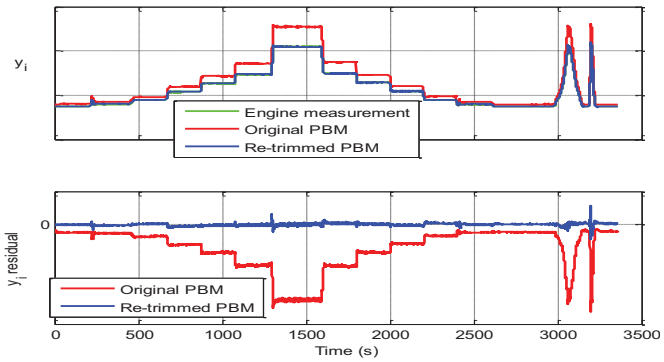

Figure 13. Nominal baseline #1

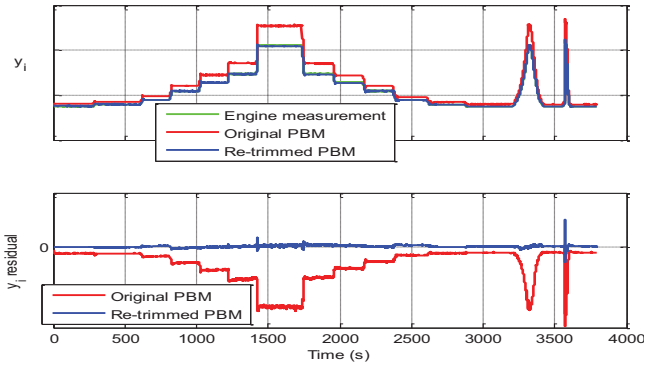

Figure 14. Nominal baseline #2

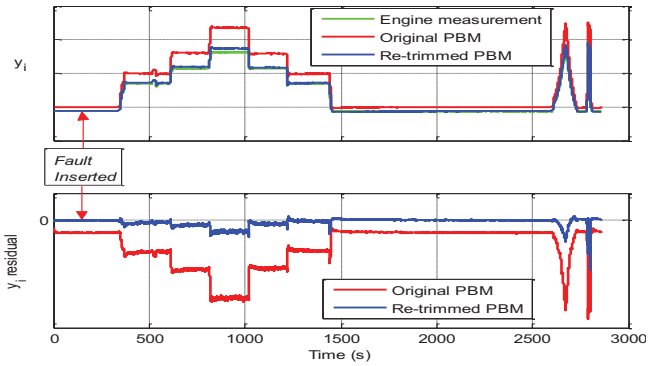

Figure 15. Station 2.5 bleed valve fault

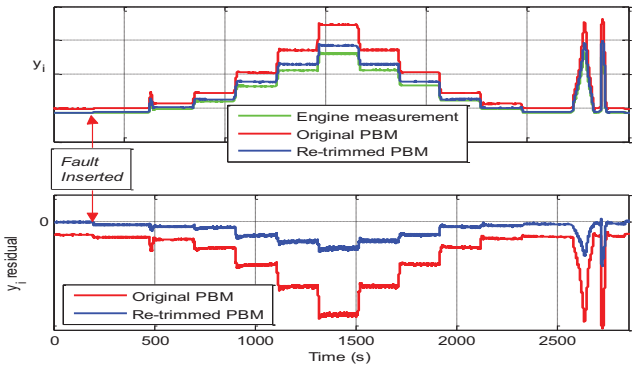

Figure 16. 14th stage bleed valve fault

Figures 15 and 16 show residual results obtained by processing two of the bleed fault cases conducted during the VIPR testing. This includes a station 2.5 bleed fault case (Fig. 15) and a 14th stage bleed fault case (Fig. 16). In each case the bleed valves were failed open. The time of fault insertion is denoted by the red vertical arrows in each figure. Once again, the top half of each figure shows the engine measurement, the original model PBM produced estimate, and the re-trimmed PBM model produced estimate of y_i while the bottom half of each figure shows the residual information for the original model and the re-trimmed model. In cases such as these where a fault is present, it is necessary for the sensed engine outputs and the PBM produced estimated outputs to diverge in order for the anomaly to be readily detectable. While the original model still exhibits large residuals in these cases we can observe that the re-trimmed model also diverges from the measured engine output, albeit to a lesser extent. For the station 2.5 bleed fault, shown in Fig. 15, the engine and the PBM agree well at lower power conditions and do not noticeably diverge until the engine reaches higher power settings. This is expected as this is a modulated bleed valve and it is normally scheduled open at low power settings and modulates closed as the engine moves to higher power settings. As such, the engine and PBM agree at lower power settings and begin to diverge as the engine increases in power. For the 14th stage bleed fault, shown in Fig. 16, the valve is normally closed under most operating conditions. For this fault case, a change in the residuals is immediately apparent as soon as the valve is failed open.

Anomaly Detection

The vector of engine sensed measurements versus PBM output residuals, $\tilde{y}$, are used to construct a weighted sum of squared residuals (WSSR) as previously shown in Eq. (3). The measurement residual matrix, R, applied within this equation was determined empirically by calculating the covariance in the residuals based on the available nominal baseline run data. The residuals used to produce the WSSR signal consist of all sensor measurements shown in Table 1, with the exception of the N1 measurement, which is used as a PBM input. Anomaly detection is then performed by comparing the WSSR signal against a defined anomaly detection threshold. If this threshold is exceeded, an anomaly is declared.

The WSSR results obtained by processing the acquired VIPR data are shown in Figs. 17-20. Here, only re-trimmed PBM results are shown. When using the original PBM it was not possible to reliably distinguish between normal and anomalous engine behavior due to the large mismatch between the engine and the model. The top half of each figure shows a time history plot of one of the measured gas path parameters (denoted as y_i) and the bottom half of the figure shows the corresponding WSSR information (blue line) and a threshold applied and monitored for anomaly detection purposes (magenta dashed line). This threshold was manually set to ensure that no false alarms were generated when processing the nominal (fault-free) engine data acquired during VIPR testing. Additionally, the WSSR signal was processed through a median

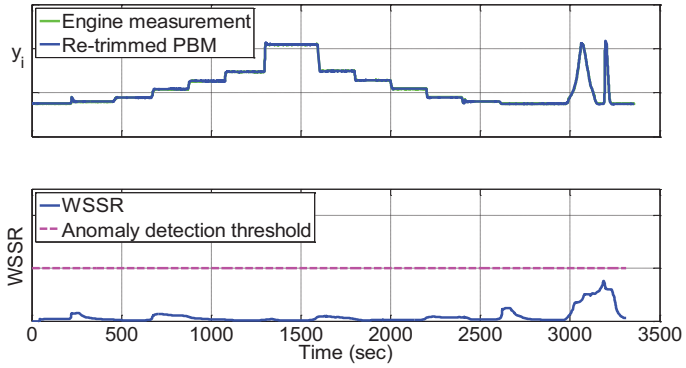

Figure 17. Nominal baseline run #1

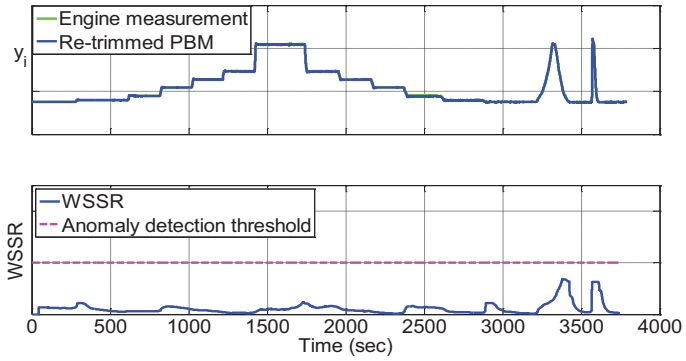

Figure 18. Nominal baseline run #2

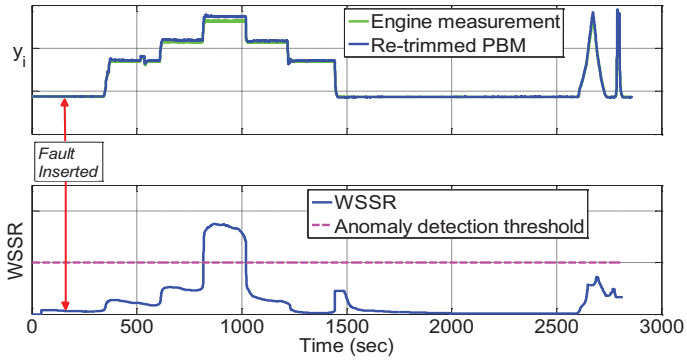

Figure 19. Station 2.5 bleed valve fault

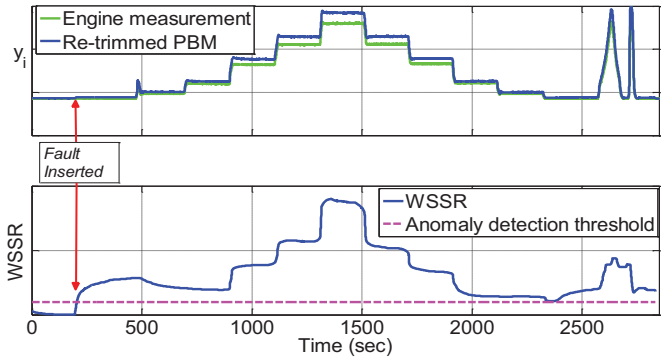

Figure 20. 14th stage bleed valve fault

filter [15] to help smooth the signal and reduce noise. The median filtered WSSR signal is shown in the plots. For the two baseline runs, shown in Figs. 17 and 18, the filtered WSSR signal remains below the threshold throughout the entire test case although increases in the WSSR are evident during transients. The two bleed valve fault cases are shown in Figs. 19 and 20. In each figure the time of fault insertion is denoted by the red vertical arrows. For the station 2.5 bleed fault case shown in Fig. 19, the WSSR signal exceeds the anomaly detection threshold when the engine is taken to higher power settings in the 900 to1000 second timeframe, which is expected as this is where the valve would normally be partially or fully closed. It is noted that the WSSR anomaly detection threshold is not exceeded during the engine transients performed around the 2600 to 2800 second timeframe even though the engine is taken to a power setting where off-nominal 2.5 bleed operation should be noticeable. This is due to the applied filtering of the WSSR signal and the magnitude of the fault-induced performance shift.

For the 14th stage bleed fault case shown in Fig. 20, the filtered WSSR signal exceeds the anomaly detection threshold soon after the fault is inserted and remains above the detection threshold throughout the remainder of the test case, including the transients towards the end of the test case. Comparing Figs. 19 and 20 it can be observed that the 14th stage bleed valve fault has a larger impact on engine performance than the station 2.5 bleed fault, making it more readily detectable.

RTSTM Kalman Filter Tuning Parameter Estimation

Like the PBM, the RTSTM was also updated to use the re-trimmed piecewise linear model. The Kalman filter implemented within the RTSTM estimates model state variables plus six model tuning parameters. Figures 21-24 show the RTSTM-produced tuning parameter estimates for the various test cases. In each figure the top subplot shows results using the original model and the bottom subplot shows results using the re-trimmed model. Although units have been removed, the y-axis scales are identical in all subplots. For the baseline runs, shown in Figs. 21-22, it is observed that the original model tuner estimates are larger and undergo notable variation as the engine transitions to different operating points. Conversely, the revised model tuning parameter estimates are mainly concentrated near zero, although they do exhibit variation when the engine undergoes a transient. These results demonstrate that the re-trimmed model more accurately matches the steady-state performance of the actual engine, thus requiring smaller RTSTM tuning parameter adjustments. The station 2.5 and 14th stage bleed fault cases are shown in Fig. 23 and Fig. 24, respectively. Again, the re-trimmed RTSTM produces smaller magnitude tuners with less variation compared to the original model. While the station 2.5 bleed valve fault results in minimal variation in the tuner estimates, changes in the tuner estimates associated with the 14th stage bleed valve fault are evident, again due to the fact that the latter fault has a larger impact on engine performance. The 14th stage

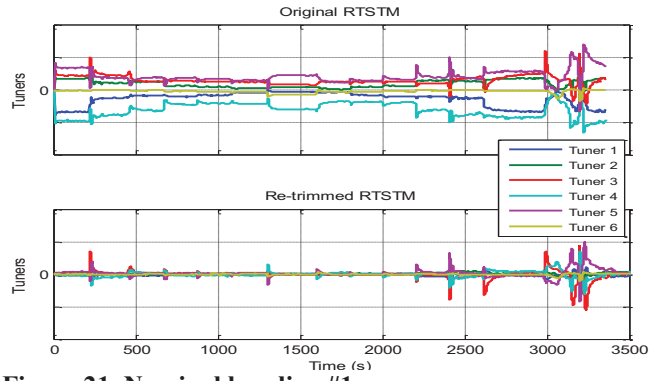

Figure 21. Nominal baseline #1

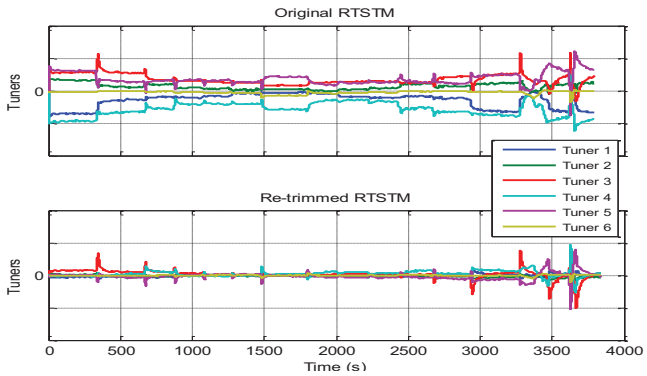

Figure 22. Nominal baseline #2

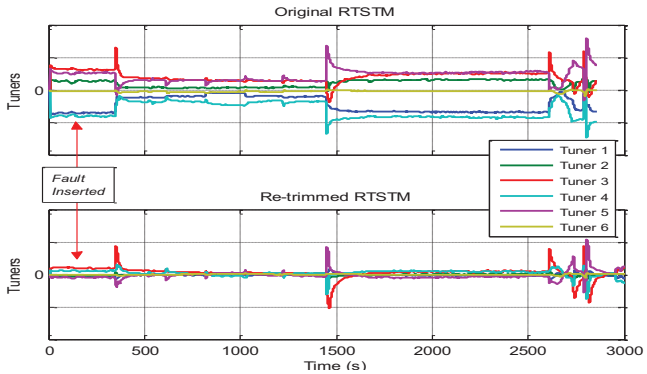

Figure 23. Station 2.5 bleed valve fault

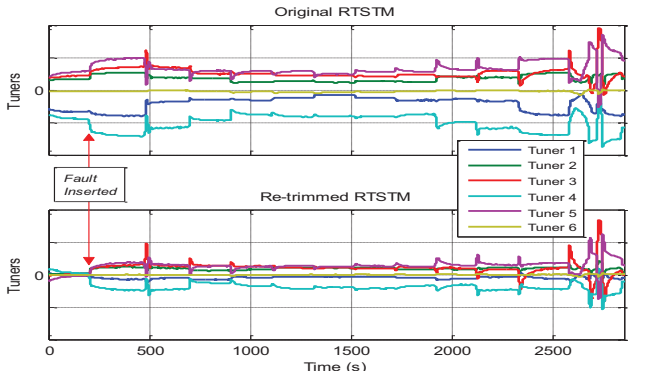

Figure 24. 14th stage bleed valve fault

bleed valve fault causes a distinct change in the estimates initiating at the time of fault insertion and remaining for the duration of the run.

DISCUSSION

The model-based anomaly detection architecture has been shown to hold promise for the processing of streaming aircraft engine measurement data. However, future maturation and enhancements are warranted. One necessary enhancement is the need to further improve engine-to-model matching specifically during engine transients. Current work is ongoing to update metal temperature state dynamics contained in the model.

It is also necessary to include and evaluate the full functionality of the architecture. The results presented in this paper exclusively focus on the anomaly detection performance achieved by updating the architecture to use a PWLM re-trimmed to match nominal engine performance. Here, the model-tuning parameters that the PBM periodically accepts from the RTSTM to reflect deterioration have been set to zero. Follow-on work is necessary to evaluate how the system will perform when the engine begins to experience performance degradation over time and model tuning parameter updates passing from the RTSTM to the PBM are necessary. Furthermore, the results presented in this paper only focus on anomaly detection capabilities. Follow-on work is ongoing to also include fault isolation logic that classifies the root cause for any detected anomalies. This will be performed by analyzing the observed residual vector present when any anomaly is detected, and then classifying the most likely root cause for the event.

SUMMARY

This paper presented a model-based anomaly detection architecture designed for the processing of aircraft engine flight data either on-board or post-flight. The significance of this technique is that it enables processing of streaming engine measurement data and the detection of fault conditions with reduced latency. The architecture has been demonstrated for processing actual engine measurement data and found to avoid false alarms and correctly detect actuator bleed fault scenarios contained within the data. A method for re-trimming the model contained within the architecture was presented and found to be an effective means of addressing model-to-engine mismatch. This was performed by fitting a polynomial curve to identified nominal engine steady-state operating data, and then updating piecewise linear model trim point information. Follow on work is recommended to further improve the transient response matching of the model and to evaluate overall architecture performance when applied to additional aircraft engine datasets.

ACKNOWLEDGMENTS

This work was conducted under the NASA Aviation Safety Program, Vehicle Systems Safety Technologies Project.

REFERENCES

[1] Federal Aviation Administration, 2004, "Flight Operational Quality Assurance," Advisory Circular AC120-82.

[2] Civil Aviation Administration, 2003, "Flight Data Monitoring—A Guide to Good Practice," Civil Aviation Publication CAP739.

[3] Gorinevsky, D., Matthews, B., Martin, R., (2012), "Aircraft Anomaly Detection using Performance Models Trained on Fleet Data," IEEE 2012 Conference on Intelligent Data Understanding. Boulder, CO, Oct. 24-26.

[4] Chu, E., Gorinevsky, D., (2010), "Detecting Aircraft Performance Anomalies from Cruise Flight Data," AIAA-2010-3307, AIAA Infotech @ Aerospace Conference, Atlanta GA, April 20-22.

[5] Das, S., Sarkar, S., Ray, A., Srivastava, A., Simon, D., (2013), "Anomaly Detection in Flight Recorder Data: A Dynamic Data-Driven Approach," Proceedings American Control Conference, pgs. 2668-2673, Washington, DC, June 17-19.

[6] Merrington, G., Oh-Kyu, K., Goodwin, G., Carlsson, B., "Fault Detection and Diagnosis in Gas Turbines," ASME Journal of Engineering for Gas Turbines and Power, Vol. 113, pp. 276-282.

[7] Kerr, L. J., Nemec, T.S., Gallops, G. W., (1991), "Real-Time Estimation of Gas Turbine Engine Damage Using a Control Based Kalman Filter Algorithm," 91-GT-216, International Gas Turbine and Aeroengine Congress and Exposition, Orlando, FL, June 3-6.

[8] Dewallef, P., Léonard, O., Mathioudakis, K., (2004), "On-Line Aircraft Engine Diagnostics Using a Soft Constrained Kalman Filter," GT2004-53539, ASME Turbo Expo, Vienna, Austria, June 14-17.

[9] Borguet, S., Dewallef, P., Léonard, O., (2005), "On-Line Transient Engine Diagnostics in a Kalman Filtering Framework," GT2005-68013, ASME Turbo Expo Reno NV, June 6-9.

[10] Simon, D. L., (2010), "An Integrated Architecture for Onboard Aircraft Engine Performance Trend Monitoring and Gas Path Fault Diagnostics," Proceedings of The 2010 JANNAF Joint Subcomittee Meeting, Colorado Springs, CO, May 3-7.

[11] Armstrong, J.B., Simon, D.L., (2011), "Implementation of an Integrated On-Board Aircraft Engine Diagnostic Architecture," AIAA-2011-5859, 47th AIAA Joint Propulsion Conference & Exhibit, San Diego, CA, July 31-August 3.

[12] Volponi, A., (2008), "Enhanced Self-Tuning On-Board Real-Time Model (eSTORM) for Aircraft Engine Performance Health Tracking," NASA CR-2008-215272.

[13] Armstrong, J.B., Simon, D.L., (2012), "Constructing an Efficient Self-Tuning Aircraft Engine Model for Control and Health Management Applications," Annual Conference of the Prognostics and Health Management Society, Minneapolis, MN, Sep. 23-27.

[14] May, Ryan D., Csank, Jeffrey, Lavelle, T. M., Litt, Jonathan S., and Guo, Ten-Huei, (2010), "A High-Fidelity Simulation of a Generic Commercial Aircraft Engine and Controller," AIAA-2010-6630, 46th AIAA Joint Propulsion Conference and Exhibit, Nashville, TN, July 25-28.

[15] Ganguli, R., Dan, B., (2004), "Trend Shift Detection in Jet Engines Gas Path Measurements Using Cascaded Recursive Median Filter With Gradient and Laplacian Edge Detector," Journal of Engineering for Gas Turbines and Power, Vol. 126, No. 1, pp.55-61.